1 | LOCAL CHROMATIN CONFORMATION

1.1 INTRODUCTION

The Hi-C assay provides a genome-wide overview of chromatin conformation, however this broad scope as an all-vs-all assay comes with inherent limits to the resolution at which individual interactions can be analysed. For a closer look at chromatin conformation within a region of interest, alternative C-based assays such as 3C, 4C and 5C can be employed alongside classical microscopy techniques like FISH.

Here I discuss a collaborative project involving the use of 4C and 5C data to zoom in on a well-studied locus involved in limb development: the Sonic hedgehog (*Shh*) gene and its distal *cis*-regulatory element named ZRS.

1.2 THE SHH LOCUS

Anterior-posterior patterning in the developing limb is regulated in mammals by the Sonic hedgehog morphogen, encoded by the *Shh* gene.[3] Specifically, the *Shh* gene is expressed within a confined region of developing limb buds named the "zone of polarising activity" (ZPA). Its expression within this region is known to be regulated by a well-studied enhancer, the "ZPA regulatory sequence" or ZRS.[4] ZRS is located almost 1 Mb downstream of its target *Shh* promoter in humans (nearer 800 kb in mouse), and is located in intronic regions of another gene, LMBR1 (Fig. 1).[4,5] Expression of *Shh* within the ZPA is tightly controlled, initiating in mice at developmental stage E9.5 and terminating at E12.5.[6] As such, single point mutations and short insertions within the ZRS enhancer have been linked to various limb deformities, including pre- and post-axial polydactyly.[3,5,7] For example, a heritable point mutation in the ZRS enhancer is the cause of polydactyly in "Hemingway cats", a large group of domestic cats with extra toes that reside at the former home of Ernest Hemingway.[7,8]

To further investigate the dynamics of the *Shh* locus, our collaborators in the Hill lab (University of Edinburgh) have developed a model system which allows inducible *Shh* expression in a non-expressing 14fp cell line derived from the developing murine limb bud. Treatment of this cell line with the histone deacetylase inhibitor trichostatin A (TSA) then leads to detectable *Shh* expression, and increased levels of the histone activation mark H3K27ac at the ZRS (*unpublished data*). However, the question remains whether this TSA treatment is fundamentally altering local chromatin structure—that
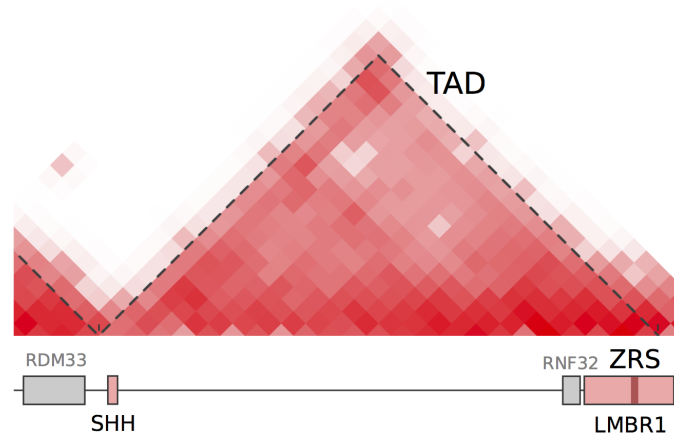
Figure 1: SHH–ZRS contacts occur within a stable TAD. An approximately 1 Mb region of the mouse genome is shown below a Hi-C contact map (derived from previously published data[1]). A clear TAD can be identified spanning from SHH to ZRS, dashed lines show TAD boundaries called by Dixon *et al.*[1]. This figure was generated for Anderson *et al.*[2].

is, bringing together the ZRS enhancer with its target *Shh* promoter—or whether ZRS and *Shh* are in contact in both the active and non-expressing cell lines in a poised state. Previous 3D-FISH experiments have shown the ZRS–*Shh* contact to be associated with *Shh* expression in the developing limb bud, though it is not detected in every cell.[4,6] Instead only a proportion of cells in the ZPA are *Shh*-expressing at a given time, and it is thought that the ZRS–*Shh* colocalisation is most likely to occur within these expressing cells.[6]

My part in this collaboration was to analyse 3C-seq (also known as 4C), then 5C data generated by our collaborators over the *Shh*–ZRS region in mouse. Experimental design and wet-lab procedures were performed by members of the Hill lab.

1.3 4C OF THE ZRS

4C experiments were performed by collaborators using the ZRS region as a bait sequence, or "viewpoint", such that ZRS contacts were measured with all other HindIII restriction fragments genome-wide. Thus the 4C technique allows us to assay changes in the ZRS–*Shh* contact relative to the totality of other chromatin interactions involving ZRS.

The 4C experimental design involved two control experiments. The first used cells derived from whole limb bud at developmental stage E11.5, thereby containing some *Shh* expressing cells as a positive control. The negative control was a mouse mandibular cell line (MD) which does not express *Shh*. Expression status in each case was experimentally verified (*data not shown*). For the perturbation experiment, 4C was

performed in the *Shh*-inducible 14fp cell line, both with and without trichostatin A (TSA) treatment.

1.3.1 4C pipeline

The 4C analysis pipeline, starting from de-multiplexed sequencing reads (`fastq` files) as produced by our in-house sequencing facilities using an Ion Torrent Ion Proton™ sequencer, can be summarised as:

1. Trim known bait sequence using `cutadapt`,[9] select only those reads where known viewpoint-associated sequence was present

2. Map reads to the mouse reference genome (build `mm9`) using `bowtie2`[10] with the `very-sensitive` flag

3. Filter alignments with a MAPQ score > 30 to select for high-confidence alignments using `samtools`[11]

4. Normalise contacts using the `r3cseq` R package and assign FDR q-values to interactions, with the aim of finding those significantly over-represented relative to expectation (Methods **??**)

1.3.2 ZRS–*Shh* interaction following TSA treatment

The results of a comparison between 4C experiments in TSA treated and untreated 14fp cells is shown in Figure 2. In it we see a striking and highly significant ZRS–SHH contact in the treated sample (q-value $< 5 \times 10^{-10}$), with a weaker but still significant contact in the adjacent restriction fragment in the untreated sample (q-value $< 5 \times 10^{-5}$).

Comparing these results with controls shows a detectable and significant ZRS–*Shh* contact in each case, regardless of *Shh* expression status (FDR q-value < 0.05; Fig. 3). This is in agreement with previous evidence suggesting ZRS contacts *Shh* constitutively.[12] However the TSA– 14fp cell line also shows a large number of off-target contacts, potentially indicating a lack of specificity in the ZRS–*Shh* contact, or a range of alternative contacts occurring throughout the cell population.

Unpublished experimental results show that following TSA treatment, *Shh* expression increases over a period of 24 hours until it reaches that seen in the limb, this steady increase is also mirrored by an increase in the level of H3K27ac histone mark over ZRS (Hill lab, *personal communication*). For this reason, 4C of ZRS was also performed a full 24 hours after TSA treatment, as well as the 18 hour treatment analysed above (e.g. Fig. 3). These two experiments give largely similar results (Fig. 4), and the ZRS–*Shh* interaction frequency is highly significant in each case, particularly
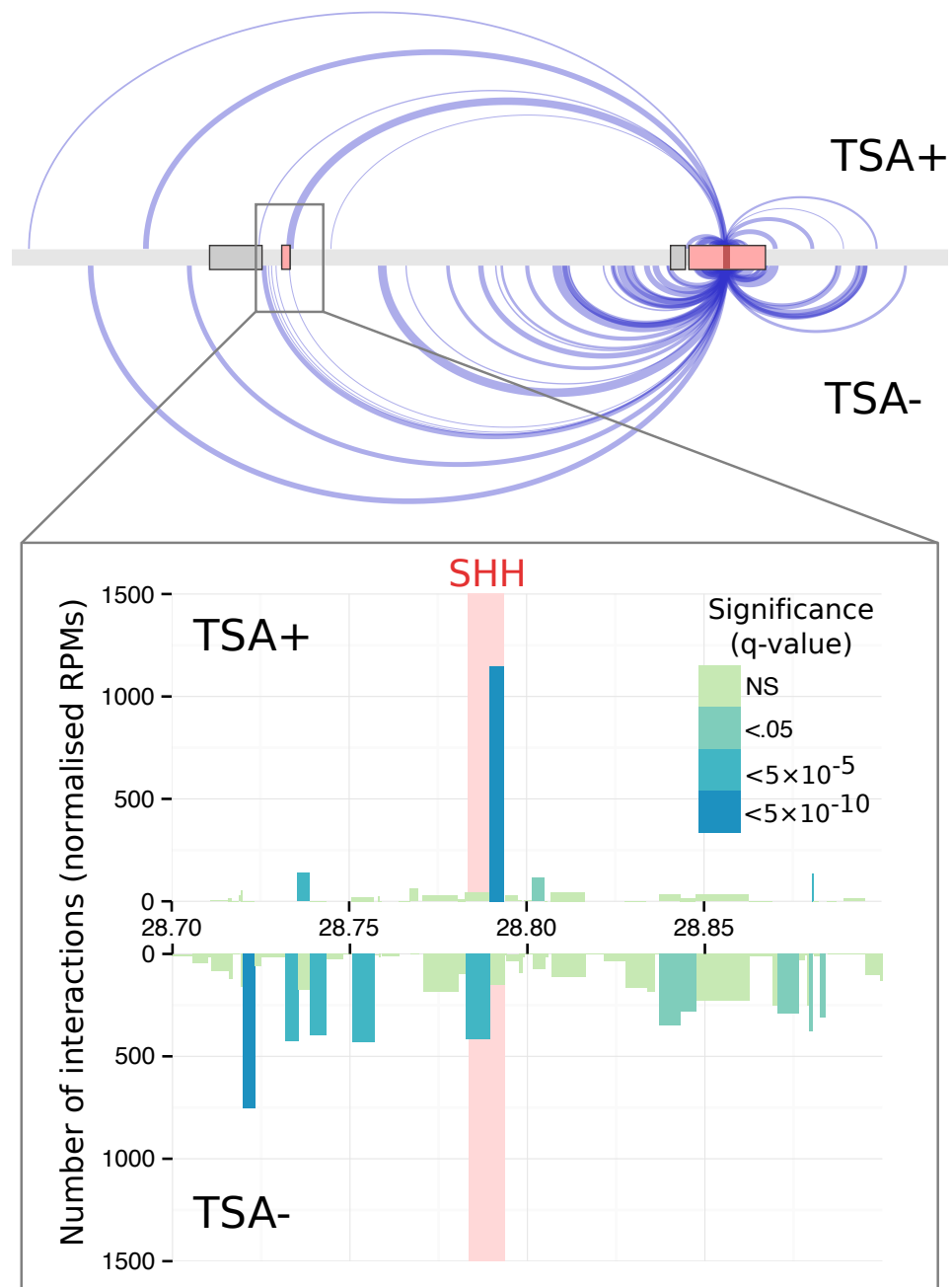
Figure 2: TSA treatment induces a strong ZRS–SHH interaction. 4C interactions are shown as edges from source node (ZRS enhancer bait fragment) to targets along an approximately 2 Mb region of chromosome 5. Edge width is proportional to the number of interactions, only highly significant interactions are shown (FDR q-value $< 5 \times 10^{-5}$). Zoomed region shows the number of interactions of the bait region with SHH in both untreated and TSA treated (after 18h) samples. Each rectangle is a restriction fragment, coloured by FDR q-value indicating the significance of the interaction above expected levels.
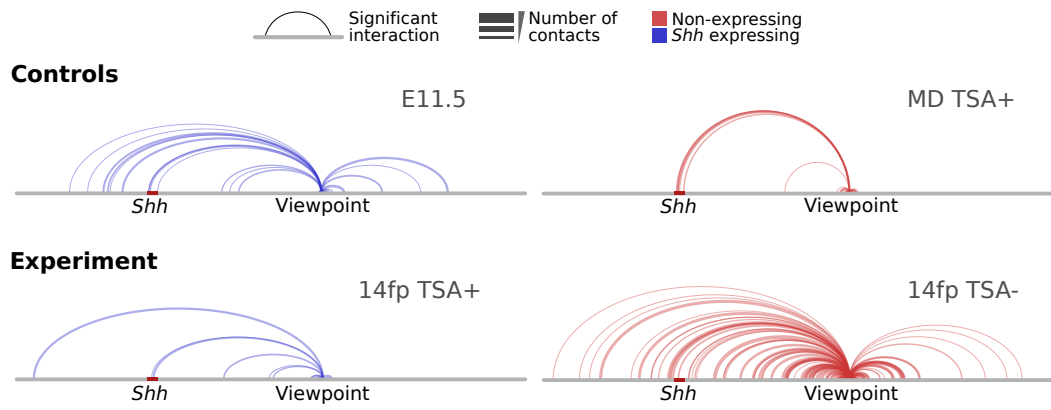
Figure 3: **TSA treatment in 14fp cells results in a more specific ZRS–*Shh* contact.** Arc plots are shown for two control experiments: the *Shh* expressing E11.5 whole limb bud and non-expressing mandibular cell line (MD). Also shown is the 14fp inducible cell line, with and without treatment with trichostatin A (TSA) after 18 hours. Arcs link significant interactions (*q*-value < 0.05) and arc widths are proportional to the normalised number of reads recorded for the interaction (Methods **??**).

24 hours after treatment (*TSA-* : $q < 1.5 \times 10^{-5}$; *TSA+*^{18h} : $q < 1.4 \times 10^{-8}$; *TSA+*^{24h} : $q < 7.8 \times 10^{-35}$).

Additional FISH data produced by our collaborators shows approximately equal levels of compaction in this region in both TSA treated and untreated 14fp cells (*data not shown*). This information in combination with the 4C results reported here (Fig. 2) support a hypothesis that as these two loci border a TAD (Fig. 1), they frequently contact each other regardless of *Shh* expression state. It could also be the case that TSA treatment brings about a more specific, functional ZRS–*Shh* contact in 14fp cells which is coupled with expression of the *Shh* gene.

1.3.3 Assay diagnostics

The 4C protocol used by our collaborators in this work was that of Stadhouders *et al.*[13] In it, the authors advise some statistical tests to ensure the quality of the experiment results. Among these were:[13]

1. Sequencing reads should be found to have high duplication rates of 95% or greater.

2. 50% or more of all reads should map to the chromosome on which the bait region is located.

Additionally, the 4C procedure was adapted for specific in-house sequencing instruments (an Ion Torrent Ion Proton™ sequencer as opposed to Illumina™ technology) and as such required diagnostics to confirm the experimental data was accurate.
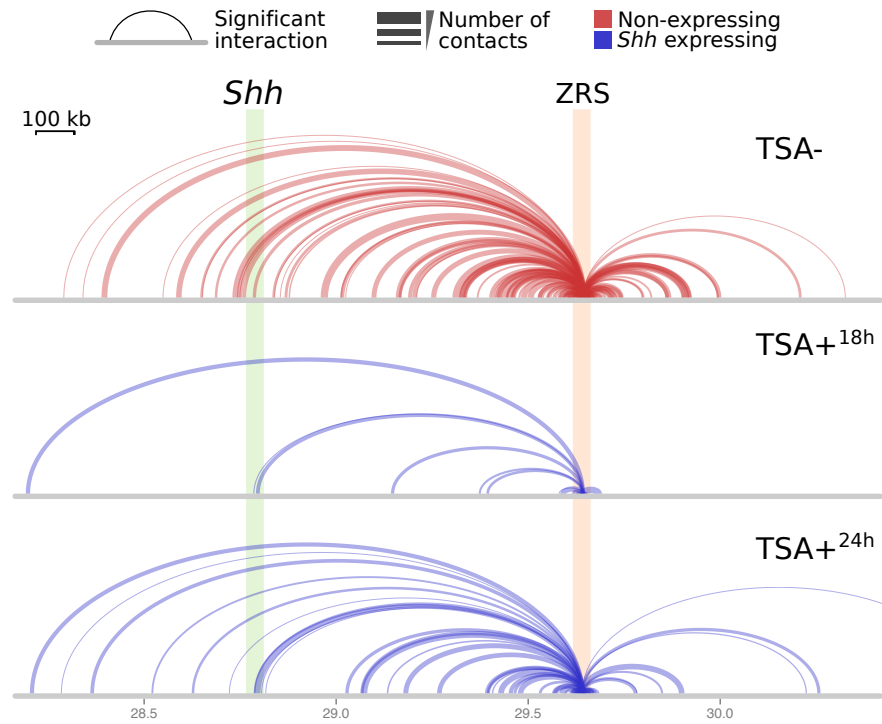
Figure 4: A stable ZRS–SHH interaction is coupled with reduced extraneous contacts. Arc plots are shown for an untreated, non-expressing 14fp cell population (*TSA-*) and following TSA treatment after 18 and 24 hours. Arcs link significant interactions (*q*-value < 0.05) and arc widths are proportional to the normalised number of reads recorded for the interaction (Methods **??**).

Table 1: 4C sequencing library statistics. 4C experiments are summarised as total number of reads in each experiment and the percentage of those reads labelled "duplicates". Note in 4C these duplicates are not artifactual and instead result from large numbers of contacts nearby to the viewpoint.

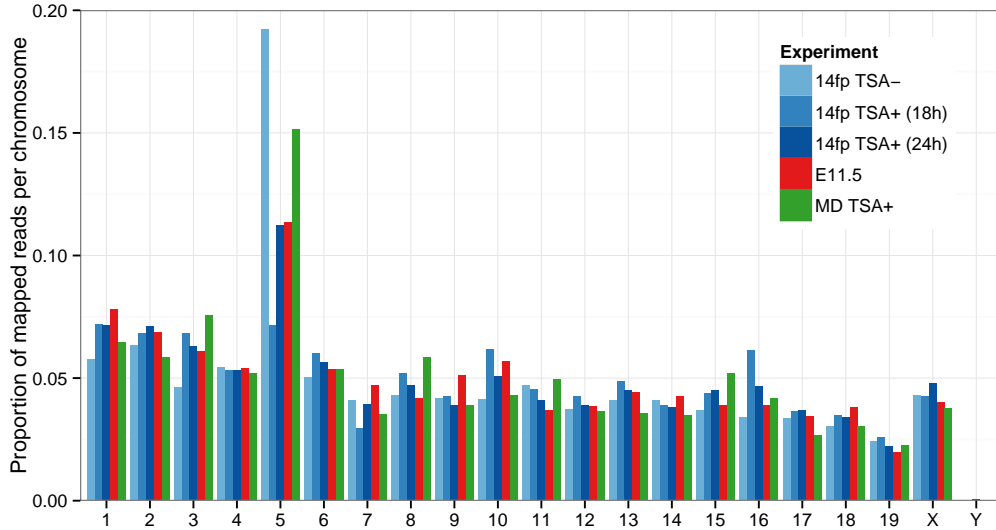|	14fp TSA-	14fp TSA+ 18h	24h	E11.5	MD TSA+
Reads (million)	10.0	8.8	24.2	10.7	12.2
Duplicated (%)	62.8	74.2	84.4	80.2	72.8

Figure 5: The bait chromosome is enriched for 4C sequencing reads. Chromosome 5 is visibly enriched for 4C reads as it contains the ZRS bait region (or viewpoint). Experiments include treated and untreated 14fp cells (TSA-, TSA+^{18h}, TSA+^{24h}) as well as positive control (E11.5) and negative control (MD TSA+).

Sequence duplication levels were measured with FastQC[14] and are shown in Table 1. We find slightly lower than expected levels of duplication, ranging from 62.8% to 84.4%. This suggests that while the assay does appear to be working, there may be extraneous noise and non-bait interactions in the sequencing library.

Second, we found the proportion of reads mapped to the bait region chromosome, chromosome 5 in this case, fell below the prescribed level of 50%. Across 4C experiments, we find instead that between approximately 10–20% of all reads mapped to the bait chromosome (Fig. 5), except for the 18 hour TSA+ treatment experiment which shows only around 7%. While this is still a clear enrichment over non-bait chromosomes, relative to their lengths, it suggests the assay results suffer from either increased *trans*-contact noise or decreased *cis*-contact enrichment around the bait region.

Lower than expected levels of both sequence duplication and bait chromosome enrichment suggest loss of signal around the bait region itself. This is the area where we expect both very high levels of duplication (identical restriction fragment pairings

between nearby genomic locations) and where a majority of all sequencing reads should originate, driving the overall chromosome enrichment seen in Figure 5. The precise reason for the discrepancy is unclear but suggests the results of the assays performed by collaborators may have a lower signal-to-noise ratio than has previously been achievable in 4C experiments.[13] Potentially the signal-to-noise ratio could be improved by utilising a double cross-linking procedure such as that used in Lin *et al.*[15]

1.4 POLYMER MODELLING

Chromosome conformation capture assays permit the exploration of genome organisation, but such data are commonly analysed using one or two-dimensional representations. A growing set of algorithms looks instead to rebuild the three-dimensional trajectory of a chromatin fibre, using Hi-C or 5C data as input (e.g. 16–23). Intuitively, in each method the interaction frequency between two regions is idealised as inversely proportional to their physical distance (and adjusted according to various other constraints). Where these methods differ is in their approaches to performing this spatial transformation, and in solving the subsequent optimisation problem. We chose the `AutoChrom3D` method[21] for use in this work (described in Section 1.4.1) as the algorithm can accept 5C input and model polymers at high resolutions of up to 8 kb.

1.4.1 AutoChrom3D method

The procedure implemented in `AutoChrom3D` can be summarised as:[21]

1. The chromatin fibre is represented as beads-on-a-string, with $N_{beads} = \lceil \frac{L}{R} \rceil$ (where L is the length of the region and R the resolution)

2. A local compaction parameter is calculated using a sliding window of each 50 adjacent beads (intra-window contacts are averaged and compared to those over the whole region under study)

3. Interaction frequency between beads of a given genomic distance is modelled as a Poisson-distributed random variable and noisy or unstable contacts, considered in the context of neighbouring beads, are filtered

4. This filtered set of interaction frequencies are then normalised using the previously-calculated compaction parameter to give an $N_{beads} \times N_{beads}$ matrix of interaction strengths

Table 2: Measurement distances between ZRS and SHH in each inferred 3D structure. Distances are given in arbitrary units. *Shh* spans two beads of the polymer model, hence two distances are calculated in each case (d_1, d_2). RMSD is the minimised root mean squared deviation between the two structures and is given as a relative unitless quantity. The radius of gyration (gyradius) is also shown.

		Distance		RMSD	Gyradius (μm)	
		TSA-	TSA+		TSA-	TSA+
88fp	d_1	5.4	5.1	1.701	0.244	0.244
	d_2	4.1	3.9			
MD	d_1	6.2	3.3	2.377	0.217	0.205
	d_2	4.8	2.0			

5. Interaction strength is converted to spatial distance through two linear transformations based on experimental observations of nuclear occupancy and regional flexibility[24]

6. Cartesian co-ordinates are then calculated via non-linear constrained optimisation of pairwise spatial distances using LINGO[25]

1.4.2 Modelling the *Shh* region with 5C

5C data was generated by our collaborators over the same ZRS–*Shh* region as was assayed with 4C (Fig. 1; Section 1.3) with the aim of developing a multi-point perspective on local chromatin conformation beyond that available from 4C data.

We used this 5C experimental data in combination with the `AutoChrom3D` three-dimensional inference algorithm[21] in an attempt to compare polymer trajectories in TSA treated and untreated 88fp mouse cells, a similar and complimentary cell line to that used in earlier 4C experiments (14fp). As a control, 5C was also performed on mandibular (MD) cells, with and without TSA treatment, which do not express *Shh*. Prior to structural modelling, the `my5C` program was used to generate normalised 5C interaction frequencies.[26]

We find that TSA treatment of 88fp cells does appear to slightly reduce the distance between *Shh* and ZRS in inferred 3D structures (Fig. 6), however this difference is overshadowed—to our surprise—by that observed in the non-expressing MD cell line. This latter mandibular cell line undergoes a large structural transition which brings the *Shh* gene and ZRS into close proximity. Measurements between these elements for each structure are shown in Table 2.

We also report a greater overall structural shift following TSA treatment in the MD cell line, with an RMSD between the two structures of 2.377 arbitrary units, relative to 1.701 between TSA+ and TSA- 88fp cells. The radius of gyration, unchanged in 88fp, is also decreased in the MD cell line following TSA treatment, indicating the region becomes more compact following TSA treatment (Table 2).
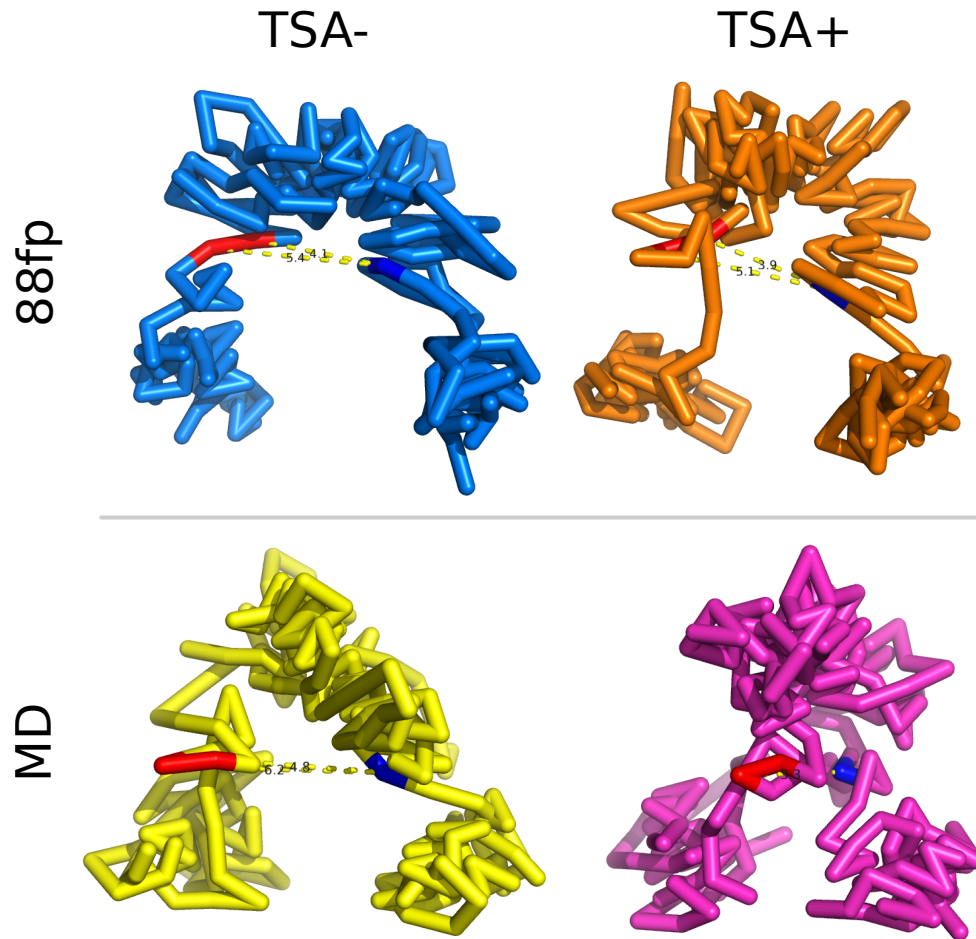
Figure 6: Inferred polymer trajectories of the ZRS–SHH region following TSA treatment in two cell lines. 3D structures are shown for 5C experiments assaying the region around *Shh* (*red*) and ZRS (*blue*) in an *Shh*-expressing limb bud cell line (88fp) and a non-expressing mandibular cell line (MD). Labelled measurements are given in Table 2. Structures were predicted by `AutoChrom3D`[21] using 210×8 kb beads per polymer.

1.4.3 Repeat simulations

We have shown what appears to be a structural shift in the ZRS–*Shh* locus per 3D modelling predictions (Section 1.4.2). It is of interest to assess the stability and reproducibility of these results through repeat simulations of the polymer trajectory. At this point it is unclear whether the ZRS–*Shh* bound state represents a firm consensus over the cell population, or an alternative structure with similar optimisation energy to that of the non-contacting state.

We re-ran simulations of the 3D chromatin fibre in the ZRS–*Shh* region a total of five times (Fig. 7). In each case, the algorithm generates the known ZRS–*Shh* TAD as a compacted domain bookended by the two loci under study. This sanity check shows that the results are broadly compatible with our *a prior* expectation of the region's structure given the 2D heatmap representation of 5C data (Fig. 1).

Repeat simulations indeed appear to recreate the induced ZRS–*Shh* contact in the mandibular cell line (MD) following TSA treatment (Fig. 7). This is again surprising, as the MD cell lines do not express *Shh* and so were included as a negative control, with no expected changes in local chromatin structure following TSA treatment. In repeat simulations of the 88fp cell line, a close analogue of the 14fp cell line used in 4C, we see relatively little change in distance between *Shh* and ZRS (Fig. 7).

We quantified these distances by measuring form the single bead containing ZRS to the two beads which overlap the *Shh* gene (Fig. 8). While these are not biological replicates, just repeat simulations, we find the distance shift in MD cells is statistically significant at the level of $\alpha = 0.05$ for both bead distances (Mann-Whitney: $d_1 : p < 0.012$, $d_2 : p < 0.012$). Distances in the 88fp cell line were not significantly different following TSA treatment (Fig. 8).

Qualitatively, there could be some observable structural dynamics caused by TSA treatment in 88fp cells. It appears potentially that part of the *Shh*–ZRS TAD becomes more loosely-packed at the ZRS side. This can be seen most clearly in two of the five simulations of the TSA treated 88fp polymer models (Fig. 9). Given the function of TSA as a histone deacetylase inhibitor, and unpublished results showing it causes an increase in H3K27 acetylation over the ZRS, we speculate that additional acetyl groups around this locus could be causing greater repulsion between histones leading to a less-compacted structure. Potentially then, the ZRS is transitioning to a more accessible state despite no change in its physical distance relative to *Shh*.

The main result, that TSA treatment induces a *Shh*–ZRS contact in mandibular cell lines but not in limb bud, is difficult to explain and runs contrary to our expectations. 4C experiments performed over the same region reported ZRS–*Shh* contacts (Fig. 4) but polymer models using 5C found instead that these two loci remain relatively separated with or without TSA treatment (though still much closer than expected relative to their genomic distance; Fig. 6). One explanation for this could be the filtering method used by `AutoChrom3D` (Section 1.4.1). Highly improbably contacts are
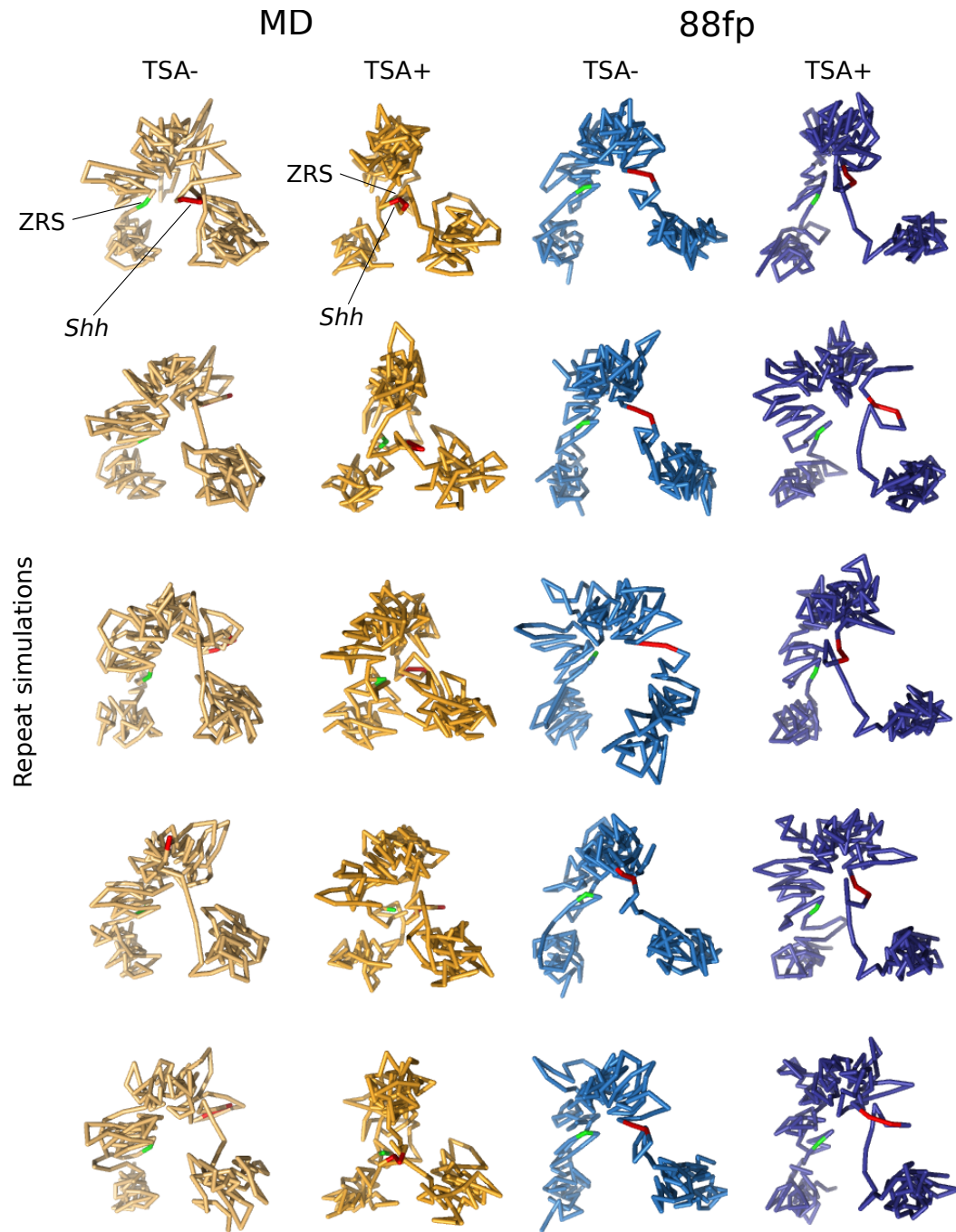
Figure 7: Repeat simulations of 3D polymer trajectories in the *Shh*–ZRS region. 3D structures are shown for 5C experiments assaying the region around *Shh* (*red*) and ZRS (*green*) in an *Shh*-expressing limb bud cell line (88fp) and a non-expressing mandibular cell line (MD). Structures were aligned as whole molecules with the uppermost replicate in each column.
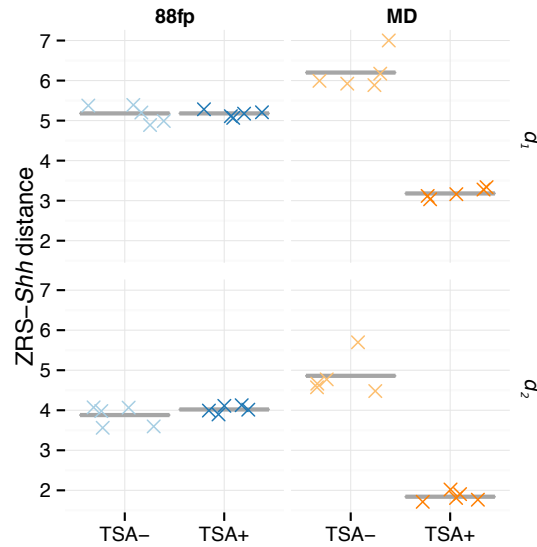
Figure 8: ZRS–*Shh* distance measurements from repeated 3D polymer simulations. Measurements were taken from 5 replicate 3D simulations (shown in Fig. 7). Distances are given in arbitrary units. *Shh* spans two beads of the polymer model, hence two distances are calculated in each case (d_1, d_2).
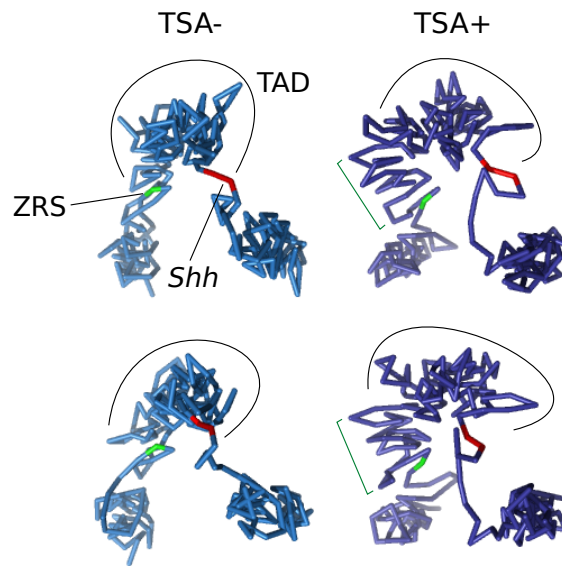

Figure 9: Polymer models showing partial TAD decompaction following TSA treatment. Two of the simulations from Figure 7 are shown here and annotated. In the TSA treated 14fp samples (TSA+) there is potentially evidence for a looser packing of the chromatin around ZRS (*dark green*).

filtered before structural prediction to prevent errors or artefacts leading to aberrant structures. In this case, a genuine instance of long-range *cis*-regulation may end up being down-weighted or removed before polymer modelling. Alternatively this may be an example of where, as has been noted at high-resolution, the results of 5C as formaldehyde cross-linking efficiencies cannot be interpreted as spatial distances.[27]

Additional follow-up experiments are underway to further explore the dynamics in this region.

REFERENCES

[1] Dixon JR, Selvaraj S, Yue F, Kim A, Li Y, Shen Y, Hu M, Liu JS, Ren B (2012) Topological domains in mammalian genomes identified by analysis of chromatin interactions. *Nature*, **485**(7398): 376–80.

[2] Anderson E, Devenney PS, Hill RE, Lettice La (2014) Mapping the Shh long-range regulatory domain. *Development (Cambridge, England)*, (September): 1–10.

[3] Anderson E, Peluso S, Lettice La, Hill RE (2012) Human limb abnormalities caused by disruption of hedgehog signaling. *Trends in Genetics*, **28**(8): 364–373.

[4] Hill RE, Lettice La, B PTRS (2013) Alterations to the remote control of Shh gene expression cause congenital abnormalities Alterations to the remote control of Shh gene expression cause congenital abnormalities Author for correspondence :. (May).

[5] Laurell T, Vandermeer JE, Wenger AM, Grigelioniene G, Nordenskjöld A, Arner M, Ekblom AG, Bejerano G, Ahituv N, Nordgren A (2012) A novel 13 base pair insertion in the sonic hedgehog ZRS limb enhancer (ZRS/LMBR1) causes preaxial polydactyly with triphalangeal thumb. *Human Mutation*, **33**(7): 1063–1066.

[6] Amano T, Sagai T, Tanabe H, Mizushina Y, Nakazawa H, Shiroishi T (2009) Chromosomal Dynamics at the Shh Locus: Limb Bud-Specific Differential Regulation of Competence and Active Transcription. *Developmental Cell*, **16**(1): 47–57.

[7] Lettice La, Hill AE, Devenney PS, Hill RE (2008) Point mutations in a distant sonic hedgehog cis-regulator generate a variable regulatory output responsible for preaxial polydactyly. *Human Molecular Genetics*, **17**(7): 978–985.

[8] Zeller R, López-Ríos J, Zuniga A (2009) Vertebrate limb bud development: moving towards integrative analysis of organogenesis. *Nature reviews. Genetics*, **10**(12): 845–858.

[9] Martin M (2011) Cutadapt removes adapter sequences from high-throughput sequencing reads. *EMBnet.journal*, **17**(1): 10–12.

[10] Langmead B, Salzberg SL (2012) Fast gapped-read alignment with Bowtie 2. *Nature methods*, **9**(4): 357–9.

[11] Li H, Handsaker B, Wysoker A, Fennell T, Ruan J, Homer N, Marth G, Abecasis G, Durbin R (2009) The Sequence Alignment/Map format and SAMtools. *Bioinformatics*, **25**(16): 2078–2079.

[12] Bouwman BA, de Laat W (2015) Getting the genome in shape: the formation of loops, domains and compartments. *Genome Biology*, **16**(1): 154.

[13] Stadhouders R, Kolovos P, Brouwer R, Zuin J, van den Heuvel A, Kockx C, Palstra RJ, Wendt KS, Grosveld F, *et al.* (2013) Multiplexed chromosome conformation capture

sequencing for rapid genome-scale high-resolution detection of long-range chromatin interactions. *Nature protocols*, **8**(3): 509–24.

[14] Andrews S (2015) FastQC (v0.10.1): A quality control tool for high throughput sequence data.

[15] Lin YC, Benner C, Mansson R, Heinz S, Miyazaki K, Miyazaki M, Chandra V, Bossen C, Glass CK, Murre C (2012) Global changes in the nuclear positioning of genes and intra- and interdomain genomic interactions that orchestrate B cell fate. *Nature immunology*, **13**(12): 1196–204.

[16] Baù D, Sanyal A, Lajoie BR, Capriotti E, Byron M, Lawrence JB, Dekker J, Marti-Renom Ma (2011) The three-dimensional folding of the α-globin gene domain reveals formation of chromatin globules. *Nature structural & molecular biology*, **18**(1): 107–14.

[17] Hu M, Deng K, Qin Z, Dixon J, Selvaraj S, Fang J, Ren B, Liu JS (2013) Bayesian inference of spatial organizations of chromosomes. *PLoS computational biology*, **9**(1): e1002893.

[18] Varoquaux N, Ay F, Noble WS, Vert Jp (2014) A statistical approach for inferring the 3D structure of the genome. *Bioinformatics (Oxford, England)*, **30**(12): i26–i33.

[19] Lesne A, Riposo J, Roger P, Cournac A, Mozziconacci J (2014) 3D genome reconstruction from chromosomal contacts. *Nature methods*, (september).

[20] Trieu T, Cheng J (2014) Large-scale reconstruction of 3D structures of human chromosomes from chromosomal contact data. *Nucleic Acids Research*, **42**(7): 1–11.

[21] Peng C, Fu LY, Dong PF, Deng ZL, Li JX, Wang XT, Zhang HY (2013) The sequencing bias relaxed characteristics of Hi-C derived data and implications for chromatin 3D modeling. *Nucleic Acids Research*, **41**(19).

[22] Ay F, Bunnik EM, Varoquaux N, Bol SM, Prudhomme J, Vert JP, Noble WS, Le Roch KG (2014) Three-dimensional modeling of the P. falciparum genome during the erythrocytic cycle reveals a strong connection between genome architecture and gene expression. *Genome research*.

[23] Caudai C, Salerno E, Zoppè M, Tonazzini A (2015) Inferring 3D chromatin structure using a multiscale approach based on quaternions. *BMC Bioinformatics*, **16**(1): 234.

[24] Kalhor R, Tjong H, Jayathilaka N, Alber F, Chen L (2012) Genome architectures revealed by tethered chromosome conformation capture and population-based modeling. *Nature biotechnology*, **30**(1): 90–8.

[25] LINDO (2015) LINGO (v15.0): Optimization modeling software for linear, nonlinear, and integer programming.

[26] Lajoie BR, van Berkum NL, Sanyal A, Dekker J (2009) My5C: web tools for chromosome conformation capture studies. *Nature methods*, **6**(10): 690–691.

[27] Williamson I, Berlivet S, Eskeland R, Boyle S, Illingworth RS, Paquette D, Bickmore WA (2014) Spatial genome organization: contrasting views from chromosome conformation capture and fluorescence in situ hybridization. pp. 2778–2791.